

## RADIO CONTINUUM AND RECOMBINATION LINE OBSERVATIONS OF THE POLYPOLAR PLANETARY NEBULA NGC 2440

ROBERTO VÁZQUEZ

Instituto de Astrofísica de Andalucía, CSIC, Apdo. Postal 3004, E-18080 Granada, Spain; vazquez@iaa.es

JOSÉ M. TORRELLES

Instituto de Astrofísica de Andalucía, CSIC, Apdo. Postal 3004, E-18080 Granada, Spain<sup>1</sup>

LUIS F. RODRÍGUEZ AND YOLANDA GÓMEZ

Instituto de Astronomía, UNAM, Apdo. Postal 70-264, 04510 México, D. F., Mexico; luisfr@astrosmo.unam.mx, gocy@astrosmo.unam.mx

J. ALBERTO LÓPEZ

Instituto de Astronomía, UNAM, Apdo. Postal 877, 22800 Ensenada, B. C., Mexico; jal@bufadora.astrosen.unam.mx

AND

LUIS F. MIRANDA

Instituto de Astrofísica de Andalucía, CSIC, Apdo. Postal 3004, E-18080 Granada, Spain; lfm@iaa.es

Received 1998 August 25; accepted 1998 December 1

### ABSTRACT

H92 $\alpha$  and He92 $\alpha$  recombination lines and  $\lambda$ 3.6 cm continuum observations have been carried out with the Very Large Array (synthesized beam 6"8  $\times$  4"2, PA 74°) toward the polypolar planetary nebula NGC 2440. The H92 $\alpha$  and He92 $\alpha$  lines have been detected, for the first time in this nebula, over a region of  $\theta \simeq 14''$  around its geometric center. The  $\lambda$ 3.6 cm continuum emission is detected over a region of  $\simeq 65'' \times 40''$ , similar in extent to the optical emission. Physical parameters of the nebula have been derived for the region in which the recombination lines were detected. From the line to continuum ratio, an electron temperature of  $\simeq 16,000$  K and a single ionized helium abundance  $Y^+ \simeq 0.14$  are obtained. A relative extinction map of NGC 2440 has also been obtained from the ratio of the  $\lambda$ 3.6 cm continuum and H $\alpha$  images. A higher relative extinction in the central region traces the dense and dusty environment of an apparent central "toroid." The velocity field obtained from the H92 $\alpha$  line suggests that the central toroidal structure has a distorted, noncircular shape. The polypolar characteristics of this nebula are discussed and compared with those of similar objects.

*Subject headings:* planetary nebulae: individual (NGC 2440) — radio lines: ISM

### 1. INTRODUCTION

NGC 2440 is a type I planetary nebula (PN) (Peimbert & Torres-Peimbert 1983) that has been extensively studied in the past. Its central star has evolved from a massive progenitor star (Hyung & Aller 1998) and has a high effective temperature ( $T_{\text{eff}} \simeq 2 \times 10^5$  K; Heap & Hintzen 1990). Richer, McCall, & Martin (1991) have determined nebular electron temperature ranging from  $1.0 \times 10^4$  to  $1.4 \times 10^4$  K, using different line and image ratios. Deep H $_2$  images by Latter & Hora (1997) show extended emission where filaments, clumps, and a central toroidal structure are apparent. Radio continuum emission at 2, 6, and 20 cm has been also reported toward this nebula (Rodríguez, García-Barreto, & Gómez 1985; Zijlstra, Pottasch, & Bignell 1989).

The morphology and kinematics of NGC 2440 have been studied by means of CCD optical imagery and spectroscopy (see, e.g., Louise & Pascoli 1985; Heathcote & Weller 1987; Icke, Preston, & Balick 1989; López et al. 1998, hereafter LMBH98, and references therein). In particular, LMBH98 describe this PN as polypolar, formed by a radially expanding ring or torus and three bipolar structures whose symmetry axes show different position angles (PAs) and extents, namely, PA 85° ( $\simeq 76''$ ), PA 35° ( $\simeq 50''$ ), and PA 60° ( $\simeq 23''$ ) (see Fig. 4 of LMBH98). These authors suggest that the presence of multiple bipolar outflows may be related to a

bipolar, rotating, episodic jet (BRET) type of phenomenon (see López, Vázquez, & Rodríguez 1995).

Given that the central torus described by LMBH98 should be associated with the collimation processes in NGC 2440, it is of interest to determine its physical conditions to gain a better insight into the shaping mechanisms that could have formed the different bipolar structures. Very Large Array (VLA) continuum and radio recombination line (RRL) data provide an important additional tool to study simultaneously its morphology, kinematics, and physical conditions (see, e.g., Garay, Gathier, & Rodríguez 1989; Gómez et al. 1989; Ershov & Berulis 1989; Roelfsema et al. 1991; Miranda, Torrelles, & Eiroa 1995). Therefore, with the goal of furthering the understanding on the central region of NGC 2440, we have made H92 $\alpha$  and He92 $\alpha$  RRLs and  $\lambda$ 3.6 cm continuum VLA observations toward this object.

### 2. OBSERVATIONS

The RRL observations at  $\lambda$ 3.6 cm were carried out with the VLA of the NRAO<sup>2</sup> in the DnC configuration, in two runs of 6 hr each during 1996 June 7 and 10, respectively. Observational parameters are shown in Table 1. Both the right and left circular polarizations were sampled. Calibration and further image processing were performed with

<sup>1</sup> Present address: Instituto Mediterráneo de Estudios Avanzados (CSIC-UIB), Universitat de les Illes Balears, E-07071 Palma de Mallorca, Spain; torrelles@iaa.es.

<sup>2</sup> The National Radio Astronomy Observatory is a facility of the National Science Foundation operated under cooperative agreement by Associated Universities, Inc.

TABLE 1  
OBSERVATIONAL PARAMETERS

Parameter (units)	Value
Bandwidth (MHz) .....	12.5
Number of channels (including "channel 0") .....	16
Central frequency (MHz) .....	8309.383
LSR velocity ( $\text{km s}^{-1}$ ) .....	+60
Channel width ( $\text{km s}^{-1}$ ) .....	28.2
Correlator mode .....	Normal
Flux density calibrator (adopted flux [Jy]) .....	3C 286 (5.2)
Phase calibrator (measured flux [Jy]) .....	0727-115 (2.5)

the Astronomical Image Processing System (AIPS) of the NRAO. Bandpass corrections were estimated using the source 0727-115. Self-calibration was done using the so-called channel 0 of the NGC 2440 data, which contains the central 75% of the total bandwidth. Phase and amplitude corrections as a function of time, at 10 s intervals, were then applied to the data, removing atmospheric and instrumental errors.

A  $\lambda 3.6$  cm continuum self-calibrated cleaned map of NGC 2440 was obtained from the channel 0, weighting the  $(u,v)$  data with the Briggs "robustness" parameter set to zero in order to optimize the trade-off between noise and angular resolution (see Briggs 1995), using the task IMAGR of AIPS. The resulting synthesized beam was  $6''.8 \times 4''.2$  (PA  $74^\circ$ ), while the rms noise of the map was  $\sigma_{\text{continuum}} = 47 \mu\text{Jy beam}^{-1}$ . Continuum emission was detected over a region of  $\sim 1'$  in size (see § 3.1).

RRL maps were obtained by first subtracting the continuum emission from the original visibilities using the task UVLIN (see Cornwell, Uson, & Haddad 1992) and then

using the task IMAGR of AIPS (robustness parameter was set to zero). Since the  $(u,v)$  coverage and weighting were the same, the resulting beam is identical to that obtained for the continuum map. The average rms noise level in the individual channels was  $\sigma_{\text{line}} \simeq 0.1 \text{ mJy beam}^{-1}$ , which is consistent with the expected thermal noise, given the on-source integration time.

### 3. RESULTS AND DISCUSSION

#### 3.1. Radio Continuum

Continuum emission at  $\lambda 3.6$  cm (Fig. 1a) covers a region similar in extent to the optical emission. For comparison purposes, an  $\text{H}\alpha$  image with  $10 \text{ \AA}$  FWHM obtained with the 2.1 m San Pedro Mártir UNAM telescope (instrumental settings described in LMBH98) is shown in Figure 1b.

Two maxima separated by  $\simeq 6''$  are observed in the central region of the radio continuum map (Fig. 1a). The geometric center of the nebula will be defined as the location of the middle point between these maxima, corresponding with  $\alpha(1950) = 07^{\text{h}}39^{\text{m}}41^{\text{s}}.4$ ,  $\delta(1950) = -18^\circ 05' 24''$ . The symmetry axes at PA  $60^\circ$  and PA  $35^\circ$  are apparent in this map. In particular, the PA  $60^\circ$  axis is traced by the emission of the central region (inside  $\theta \simeq 30''$ ), and it is almost perpendicular to the line joining the two central maxima (Figs. 1a and 1b). On the other hand, the PA  $35^\circ$  symmetry axis is traced by the so-called *north knot* (NK) and *south knot* (SK), pointed out by LMBH98, and which are visible in both of the radio continuum and  $\text{H}\alpha$  images (Figs. 1a and 1b). Other features seen in  $\text{H}\alpha$ , which belong to the more extended and fainter PA  $85^\circ$  bipolar lobes (see Fig. 4 of LMBH98), can be identified in the radio continuum map, but the whole structure at this particular PA is not detected at the  $3\sigma$  level ( $\simeq 0.14 \text{ mJy}$ ).

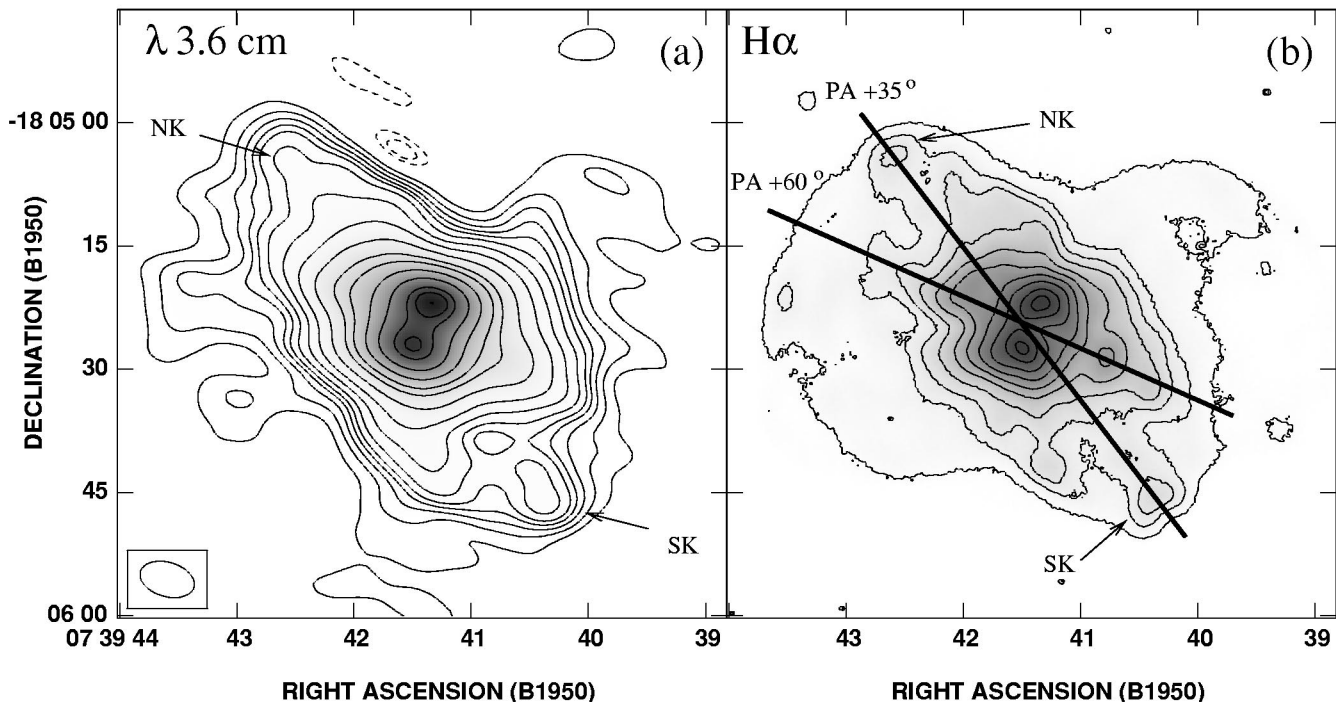


FIG. 1.—(a) Gray-scale/contour map of the radio continuum emission ( $\lambda 3.6$  cm) of NGC 2440. Contours are  $-4, -3, 3, 6, 9, 12, 15, 20, 30, 50, 100, 200, 300, 500, 800, 1200, 1400,$  and  $1590$  times  $47 \mu\text{Jy beam}^{-1}$ , the rms noise level of the map. Beam size is  $6''.8 \times 4''.2$  (PA  $74^\circ$ ), and it is shown at the lower left-hand corner. (b) Logarithmic gray-scale/contour map of the  $\text{H}\alpha$  emission shown here for comparison purposes. Levels above  $1\sigma$  were arbitrarily chosen in order to emphasize the three symmetry axes. Knots NK and SK (see text) are indicated in both figures. The axes of the outflows at PA  $60^\circ$  and PA  $35^\circ$  (see LMBH98) are also indicated.

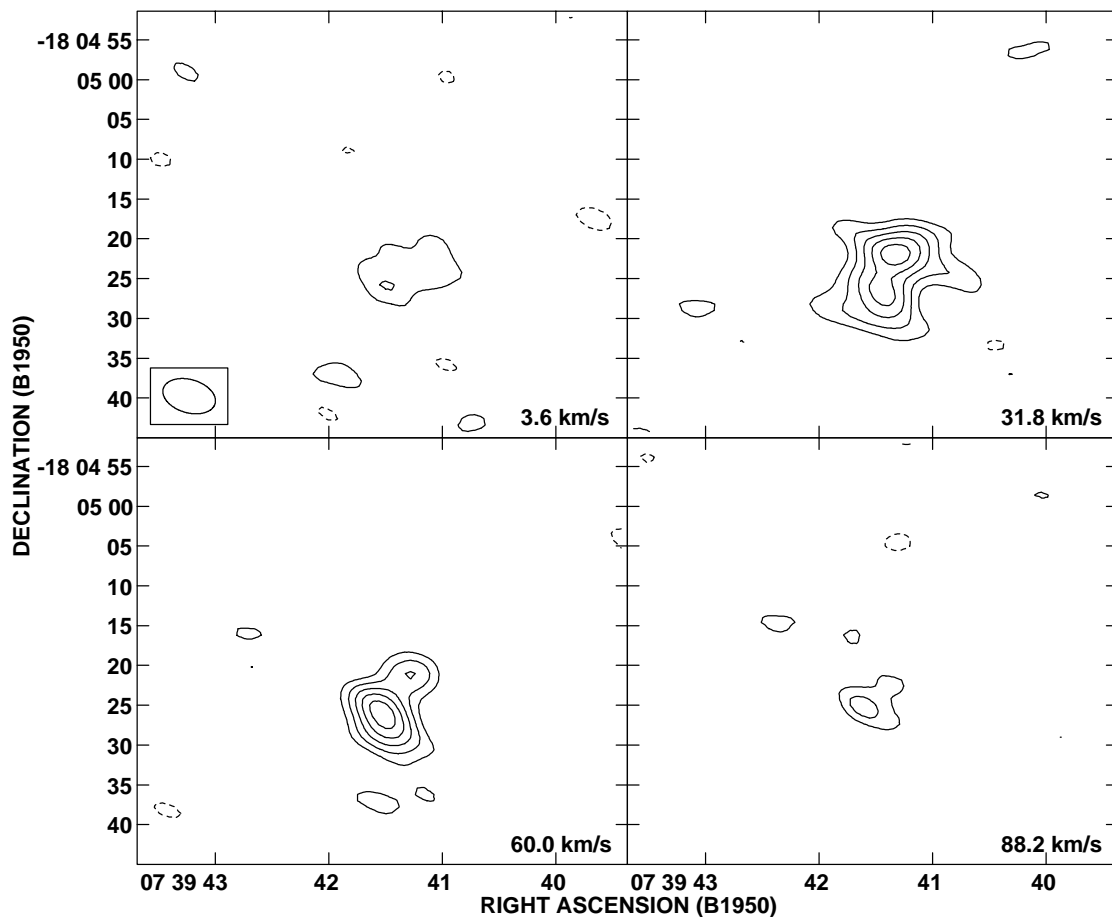


FIG. 2.—Contour maps of the individual H92 $\alpha$  velocity channels. Levels are  $-5$ ,  $-3$ ,  $3$ ,  $5$ ,  $7$ ,  $9$ , and  $11$  times  $0.1 \text{ mJy beam}^{-1}$ , the rms noise level. The  $V_{\text{LSR}}$  ( $\text{km s}^{-1}$ ) is indicated in the lower right-hand corner of each panel.

### 3.2. Radio Recombination Lines

H92 $\alpha$  emission has been detected for the first time in NGC 2440 in a region of  $\theta \simeq 14''$  around the geometric center of the nebula, coincident with the brightest regions of continuum emission. Figure 2 shows a mosaic composed of four contour maps of the individual channels where emission was detected. An integrated spectrum of the RRL emission is shown in Figure 3. This spectrum was obtained integrating, in each channel, the emission inside a box of  $\simeq 10''$ . Two emission peaks at  $V_{\text{LSR}} \simeq +40 \pm 3 \text{ km s}^{-1}$  and  $V_{\text{LSR}} \simeq -95 \pm 5 \text{ km s}^{-1}$ , as measured by a Gaussian fit, are detected. The first one corresponds to the H92 $\alpha$  line ( $S_{\text{peak}} \simeq 2.6 \text{ mJy}$ ), whereas the second one ( $S_{\text{peak}} \simeq 0.6 \text{ mJy}$ ) has been identified with the He92 $\alpha$  line, given its frequency separation from the H92 $\alpha$  maximum of  $\simeq 3.7 \text{ MHz}$ .

An integrated H92 $\alpha$  line intensity contour map is shown in Figure 4. The integration velocity range was from  $-25$  to  $+145 \text{ km s}^{-1}$ , excluding the emission from the He92 $\alpha$  line. Two maxima were found, which coincide with those in the radio continuum and H $\alpha$  images.

### 3.3. Mean Physical Parameters

Physical parameters have been derived from the region where the H92 $\alpha$  emission line is detected. Results are shown in Table 2. The relative ionized helium abundance was obtained from the He92 $\alpha$  to H92 $\alpha$  flux ratio, yielding a value  $Y^+ \simeq 0.14$ . The electron temperature ( $T_e$ ) was derived

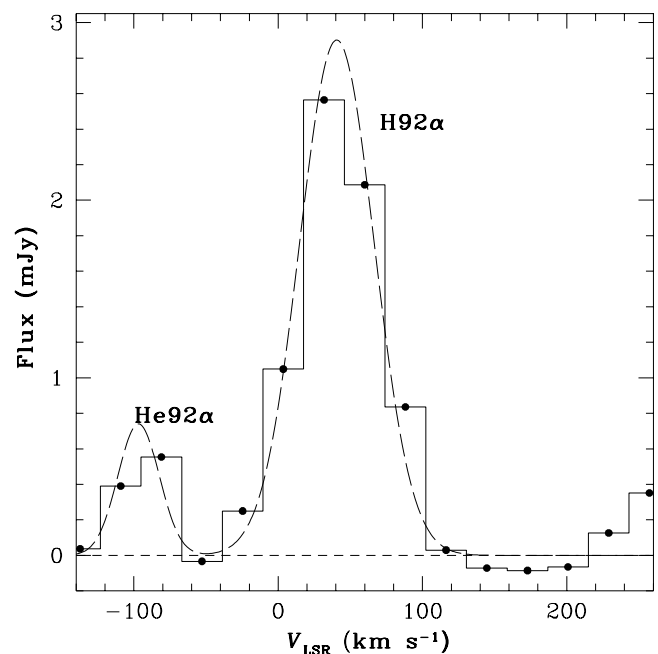


FIG. 3.—Integrated spectrum centered in the maximum of the H92 $\alpha$  line emission. Dashed line represents a Gaussian line fit to determine the velocity components. The component at  $V_{\text{LSR}} \simeq -95 \text{ km s}^{-1}$  is identified as the He92 $\alpha$  RRL, whereas the one at  $V_{\text{LSR}} \simeq 40 \text{ km s}^{-1}$  corresponds to the H92 $\alpha$  RRL.

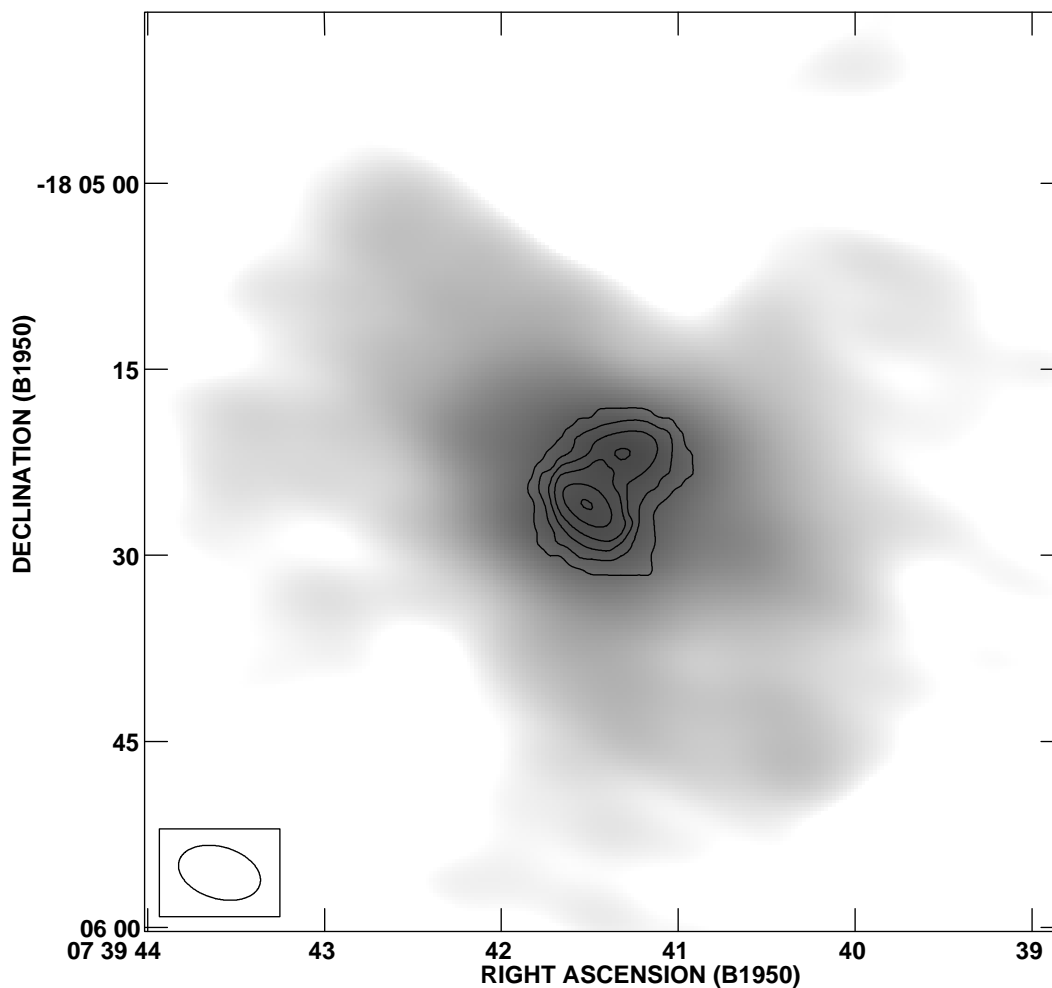


FIG. 4.—Contour map of the integrated intensity of the H92 $\alpha$  line superimposed on the  $\lambda$ 3.6 cm continuum emission (*gray-scale*). Contours are 10, 40, 55, 68, 85, and 99% of the peak (93 mJy beam $^{-1}$  km s $^{-1}$ ).

by using the equation (Roelfsema & Goss 1992)

$$T_e = \left( 6943\nu^{1.1} \frac{S_c}{S_l} \frac{1}{\Delta V_l} \frac{1}{1 + Y^+} \right)^{0.87}, \quad (1)$$

where  $\nu$  is the RRL frequency in GHz, and the other variables are described in Table 2. Non-LTE effect corrections

in temperature are negligible according with the formalism provided by Roelfsema & Goss (1992). The derived electron temperature ( $\approx 16,000$  K) is found to be in close agreement with the estimates by Richer et al. (1991) and Hyung & Aller (1998) using the [O III] lines from optical spectra.

A logarithmic  $\lambda$ 3.6 cm continuum/H $\alpha$  ratio map has been

TABLE 2  
MEAN PHYSICAL PARAMETERS

Parameter (units)	Symbol	Value
Size <sup>a</sup> (arcsec)	$\theta_{\min} \times \theta_{\text{maj}}$	10 $\times$ 11
Distance (kpc) <sup>b</sup>	$d$	1.1
$\lambda$ 3.6 cm continuum flux density (mJy)	$S_c$	170 $\pm$ 2
H92 $\alpha$ line flux density peak (mJy)	$S_l$	2.6 $\pm$ 0.1
H92 $\alpha$ line width (FWHM) (km s $^{-1}$ ) <sup>c</sup>	$\Delta V_l$	60 $\pm$ 5
He92 $\alpha$ line flux density peak (mJy)	$S_l$	0.6 $\pm$ 0.1
He92 $\alpha$ line width (FWHM) (km s $^{-1}$ ) <sup>c</sup>	$\Delta V_l$	40 $\pm$ 10
Relative ionized helium abundance by number	$Y^+$	0.14 $\pm$ 0.03
Electron temperature (K)	$T_e$	16,000 $\pm$ 1500
Electron density (cm $^{-3}$ ) <sup>d</sup>	$N_e$	3200 $\pm$ 100
Emission measure (10 $^6$ pc cm $^{-6}$ ) <sup>d</sup>	EM	0.80 $\pm$ 0.02
Systemic velocity (km s $^{-1}$ )	$V_{\text{LSR}}$	46 $\pm$ 5

<sup>a</sup> Region over which the integrated spectrum and parameters has been derived.

<sup>b</sup> Adopted distance (lower limit) from Hajian & Terzian 1996.

<sup>c</sup> Value obtained from a Gaussian fit to the spectrum.

<sup>d</sup> Following the formalism described by Mezger & Henderson 1967.

also obtained in order to estimate a point-to-point *relative* spatial extinction distribution through the nebula (Fig. 5). To produce this map, the  $H\alpha$  image from Figure 1*b* (with no flux calibration) was convolved with the beam from the radio continuum map ( $6''.8 \times 4''.2$ , PA  $74^\circ$ ), and the radio continuum map was convolved with the optical seeing ( $\theta \simeq 2''.6$ ). Both convolved images (final beam size  $7''.3 \times 4''.9$ , PA  $74^\circ$ ) were normalized to its maximum value before the ratio was obtained. A logarithmic function and then a multiplicative factor of 2.2 were applied in order to calibrate the map in magnitudes.

The values of extinction in Figure 5 are given relative to the maximum, i.e., if the absolute extinction to the maximum  $A_V(x_0, y_0)$  would be known, the full extinction map would be calibrated, as the relationship between both values is  $A_V(x, y) = A_V^{\text{rel}}(x, y) + A_V(x_0, y_0)$  [where  $A_V(x, y)$  is the absolute visual extinction in the point  $(x, y)$  and  $A_V^{\text{rel}}(x, y)$  is the corresponding relative extinction].

The relative spatial extinction map (Fig. 5) shows two maxima that roughly coincide with those in the  $\lambda 3.6$  cm continuum and  $H\alpha$  images. Extinction decreases outward from the center of the nebula, differing by up to  $\sim 0.4$  mag (equivalent hydrogen column density:  $N_{\text{H}} = 7 \times 10^{21} \text{ cm}^{-2}$ ; Spitzer 1978) between the central regions and the

farthest zones along the PA  $60^\circ$  axis. This result suggests that higher extinction traces the most dense and dusty environment of an internal (toroidal) structure. The  $\text{H}_2$  map by Latter & Hora (1997), which shows the presence of a molecular torus, or ring, and the *Hubble Space Telescope* (*HST*) image in LMBH98 support this interpretation.

It must be noted, however, that a particular reddening law should be known for NGC 2440 in order to obtain a more accurate extinction distribution in the region by means of the  $\lambda 3.6$  cm continuum/ $H\alpha$  emission ratio map (see also Bryce et al. 1997). Nevertheless, this result serves as a good qualitative indicator of the spatial extinction distribution within NGC 2440.

### 3.4. Kinematics

In order to analyze the kinematics of the central region of NGC 2440 through the  $\text{H}2\alpha$  line emission, we have obtained a set of position-velocity (PV) contour maps along different PAs from the line data cube.

Figure 6 shows two PV contour maps made along (PA  $68^\circ$ ; Fig. 6*a*) and perpendicular to (PA  $-22^\circ$ ; Fig. 6*b*) the symmetry axis defined by the central structure. Figures 6*a* and 6*b* present two distinct peak velocity components. Extended line emission covering a range of  $\simeq 120 \text{ km s}^{-1}$  at

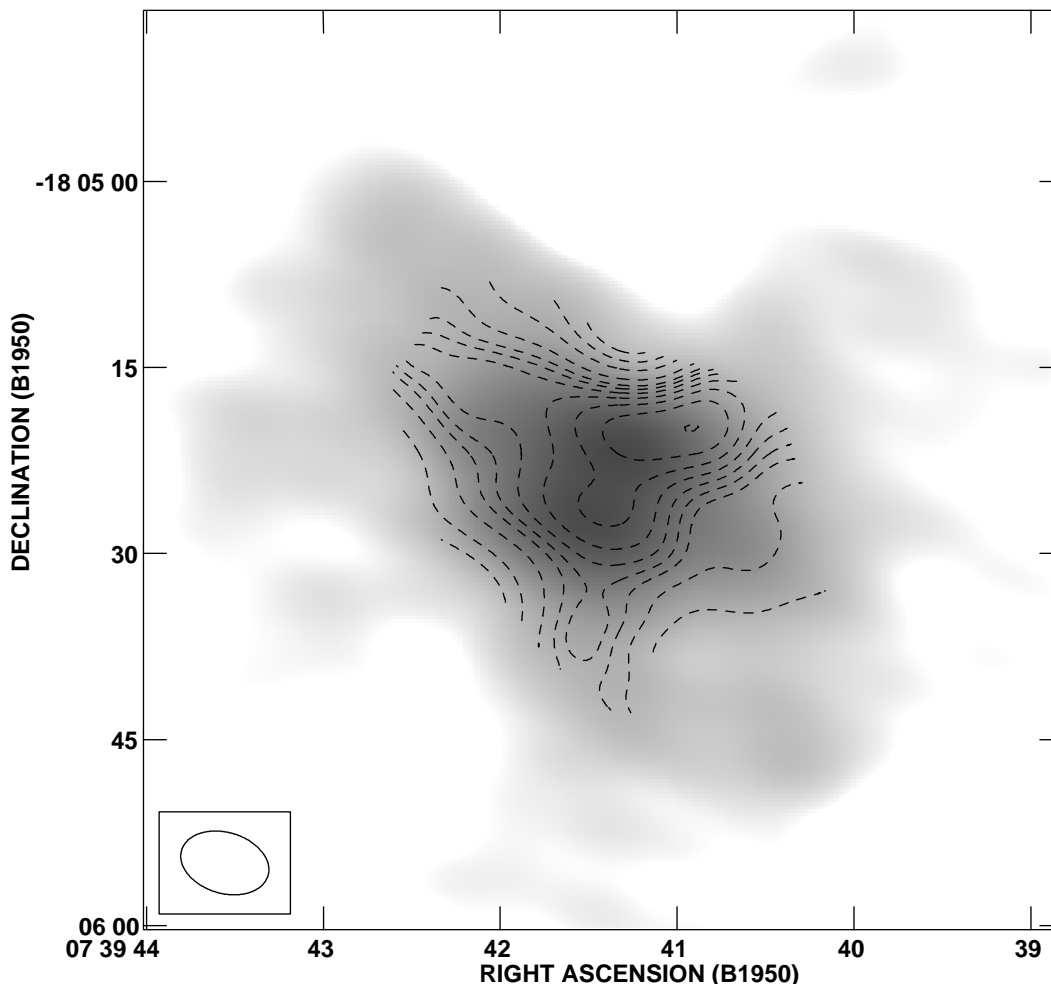


FIG. 5.—Logarithmic contour map of the radio continuum  $\lambda 3.6$  cm to  $H\alpha$  ratio superimposed on the  $\lambda 3.6$  cm continuum emission (*gray-scale*). Levels represent differential extinction (in mag) with respect to the maximum value (set arbitrarily to zero), and they are  $-1$ ,  $-0.8$ ,  $-0.6$ ,  $-0.4$ ,  $-0.3$ ,  $-0.25$ ,  $-0.2$ ,  $-0.15$ ,  $-0.1$ ,  $-0.05$ , and 0 (see text).

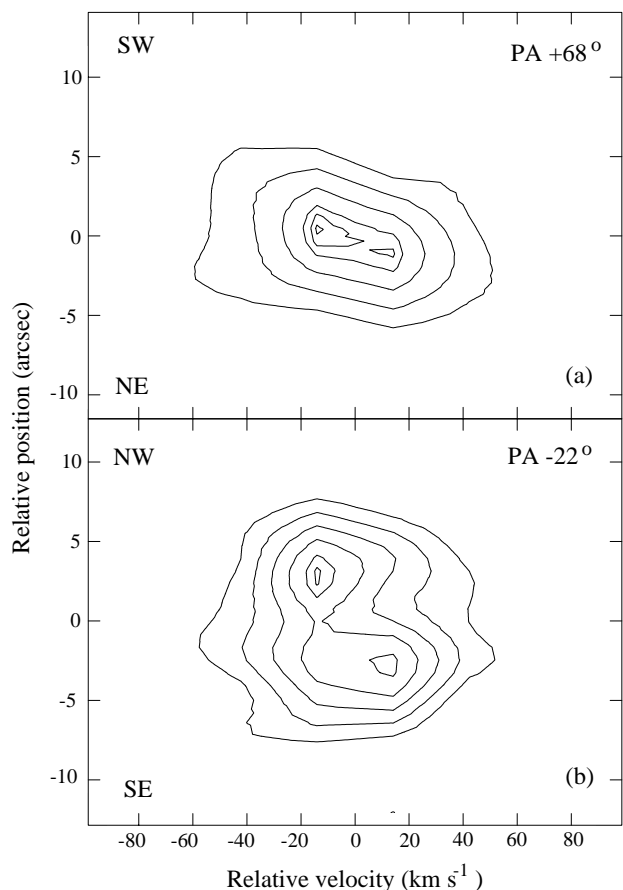


FIG. 6.—Position-velocity contour maps of two slices in the H92 $\alpha$  line data cube. (a) Slice along the symmetry axis defined by the central torus (PA 68°). Levels correspond to  $-0.5, -0.3, 0.3, 0.5, 0.7, 0.9, 1.1,$  and  $1.2$  mJy beam $^{-1}$ . (b) Slice perpendicular to the symmetry axis defined by the central torus (PA  $-22^\circ$ ). Levels correspond to  $-0.5, -0.3, 0.3, 0.5, 0.7, 0.85, 0.9,$  and  $0.95$  mJy beam $^{-1}$ . Relative positions are given with respect to the geometric center of the nebula [ $\alpha(1950) = 07^{\text{h}}39^{\text{m}}41^{\text{s}}.4,$   $\delta(1950) = -18^\circ05'24''$ ]. Relative velocities are given with respect to the systemic velocity of the PN ( $V_{\text{LSR}} = 46$  km s $^{-1}$ ).

a  $3\sigma$  level is apparent also in these maps, and this must come from the expanding regions that surround the core (see LMBH98).

The systemic velocity measured from the line splitting gives a value  $V_{\text{LSR}} \simeq +46$  km s $^{-1}$  ( $V_{\text{HEL}} \simeq +64$  km s $^{-1}$ ), which is consistent with that obtained by LMBH98.

The peak components in the PV map at PA 68° are separated by  $\sim 1''.5$  and  $28$  km s $^{-1}$ , and this would seem consistent with the kinematics expected for a slice along the axis of an expanding, tilted torus. However, for a circular ring or torus, main velocity components at zero velocity would be expected in the orthogonal cut. The PV map at PA  $-22^\circ$  shows that this is not the case. Here velocity components with the same velocity difference as those observed at PA 68° but separated by  $4''$  are observed. The global kinematics for this central region thus indicates that the western side of this structure is approaching, while the eastern side is receding. This result, together with the *HST* images presented in LMBH98 and the H $_2$  image of Latter & Hora (1997), suggests that the original shape of the toroid has been broken or distorted, probably by the erosive action of the fast stellar wind and substantial UV radiation emerging from the very hot nucleus of NGC 2440, and is now undergoing a disruption process.

#### 4. GENERAL CONSIDERATIONS

NGC 2440 is a remarkable PN. The presence of three different systems of bipolar outflows located at different position angles with distinct characteristics, such as outflow speeds and collimation conditions, precludes at present a simple dynamical interpretation.

It is interesting to notice that the orientation of the plane of the central “toroid” seems perpendicular to the bipolar subsystem located along PA 60°, thus presumably now associated with the youngest of these phenomena. However, in its present condition it lies rather off-axis with respect to the other two bipolar subsystems at PAs 85° and 35°, and it is difficult to envisage how this toroidal structure was related to their original collimation mechanism. The standard concept of equatorial enhancements located perpendicular to the bipolar outflows seems to require additional interpretations in the case of this PN with a massive, fast-evolving nucleus. This peculiar situation has also been noted to occur in the case of the extraordinary PN K $\text{jPn}$  8 by Steffen & López (1998) where the plane of a CO expanding disk found by Forveille et al. (1998) is oriented perpendicular to the most recent high-velocity bipolar jets and also far off-axis with respect to the large bipolar envelope.

The shaping of NGC 2440 seems to have been strongly influenced by episodic bipolar outflows at different orientations where the collimating agent and the equatorial regions nearest to it have suffered substantial transformations with time. In this context it is interesting to consider the case of the very young PN He 3-1357 (Bobrowsky et al. 1998), the “Stingray Nebula.” In that case, there is evidence of episodic activity in the stellar wind and *HST* images have revealed the presence of two systems of bipolar outflows with seemingly different orientations that have already been generated in an early stage of development of this object. Additional objects in this group of polypolar nebulae, such as NGC 6302 and Mz 3 (Meaburn & Walsh 1980, 1985) and those referred to as quadrupolar nebulae (Manchado, Stanghellini, & Guerrero 1996), point out the relevance that multiple collimated outflows play in PN evolution.

#### 5. CONCLUSIONS

The PN NGC 2440 has been observed with the VLA through the H92 $\alpha$  and He92 $\alpha$  lines and  $\lambda 3.6$  cm continuum. The  $\lambda 3.6$  cm continuum emission is observed over a region of  $\simeq 65'' \times 40''$ . H92 $\alpha$  and He92 $\alpha$  line emission are detected concentrated in the central region within a  $\theta \simeq 14''$  in size, where mean physical parameters have been derived, including the single ionized helium abundance ( $Y^+ \simeq 0.14$ ) and electron temperature ( $T_e \simeq 16,000$  K).

A relative extinction map has also been obtained from the logarithmic  $\lambda 3.6$  cm continuum to H $\alpha$  ratio images. Extinction is highest in the central region and along PA 60°, decreasing outward and reaching a difference of  $\sim 0.4$  mag with respect to the core.

The observed kinematics in the inner region has revealed the presence of an expanding noncircular toroidal-like structure that is probably now being disrupted by the sustained erosive action of the fast stellar wind and copious UV radiation from the very hot central star of this PN.

Polypolar nebulae conform a relevant group among planetary nebulae with multiple collimated outflows such as BRETs (see, e.g., López 1997) and point-symmetric nebulae (Guerrero, Vázquez, & López 1999). These groups denote a

fundamental stage in PN evolution in which additional information on their general properties is required for a better understanding of their origin and development.

We would like to thank Miller Goss for many useful and valuable comments on this work. R.V. is in grateful receipt of a postgraduate scholarship from the Agencia Española de Cooperación Internacional (Spain) and complementary support from DGAPA-UNAM (Mexico). L. F. M., J. M. T.,

and R. V. M. are supported in part by DGICYT grant PB95-0066 and by the Junta de Andalucía (Spain). Y. G. and L. F. R. acknowledge support from DGAPA-UNAM and CONACYT (Mexico). J. A. L. acknowledges support from DGAPA-UNAM grant IN 111896. J. M. T. acknowledges the hospitality of the Departament de Física of the Universitat de les Illes Balears (Spain) during the preparation of this paper.

## REFERENCES

- Bobrowsky, M., Sahu, K. C., Parthasarathy, M., & García-Lario, P. 1998, *Nature*, 392, 469
- Briggs, D. 1995, Ph.D. thesis, New Mexico Inst. of Mining and Technology
- Bryce, M., Pedlar, A., Muxlow, T., Thomasson, P., & Mellema, G. 1997, *MNRAS*, 284, 815
- Cornwell, T. J., Uson, J., & Haddad, N. 1992, *A&A*, 258, 583
- Ershov, A. A., & Berulis, I. I. 1989, *Soviet Astron. Lett.*, 15, 178
- Forveille, T., Huggins, P. J., Bachiller, R., & Cox, P. 1998, *ApJ*, 495, 111
- Garay, G., Gathier, R., & Rodríguez, L. F. 1989, *A&A*, 215, 101
- Gómez, Y., Rodríguez, L. F., Moran, J. M., & Garay, G. 1989, *ApJ*, 345, 862
- Guerrero, M., Vázquez, R., & López, J. A. 1999, *AJ*, in press
- Hajian, A. R., & Terzian, Y. 1996, *PASP*, 108, 419
- Heap, S. R., & Hintzen, P. 1990, *ApJ*, 353, 200
- Heathcote, S. R., & Weller, W. G. 1987, in *Late Stages of Stellar Evolution*, ed. S. Kwok & S. R. Pottasch (Dordrecht: Reidel), 411
- Hyung, S., & Aller, L. H. 1998, *PASP*, 110, 466
- Icke, V., Preston, H. L., & Balick, B. 1989, *AJ*, 97, 462
- Latter, W. B., & Hora, J. L. 1997, in *IAU Symp. 180, Planetary Nebulae*, ed. H. J. Habing & H. J. G. L. M. Lamers (Dordrecht: Kluwer), 254
- López, J. A. 1997, in *IAU Symp. 180, Planetary Nebulae*, ed. H. J. Habing & H. J. G. L. M. Lamers (Dordrecht: Kluwer), 197
- López, J. A., Meaburn, J., Bryce, M., & Holloway, A. J. 1998, *ApJ*, 493, 803 (LMBH98)
- López, J. A., Vázquez, R., & Rodríguez, L. F. 1995, *ApJ*, 455, L63
- Louise, R., & Pascoli, G. 1985, *A&A*, 150, 285
- Manchado, A., Stanghellini, L., & Guerrero, M. A. 1996, *ApJ*, 466, L95
- Meaburn, J., & Walsh, J. R. 1980, *MNRAS*, 193, 631
- . 1985, *MNRAS*, 215, 761
- Mezger, P. G., & Henderson, A. P. 1967, *ApJ*, 147, 471
- Miranda, L. F., Torrelles, J. M., & Eiroa, C. 1995, *ApJ*, 446, L39
- Peimbert, M., & Torres-Peimbert, S. 1983, in *IAU Symp. 103, Planetary Nebulae*, ed. D. R. Flower (Dordrecht: Reidel), 233
- Richer, M. G., McCall, M. L., & Martin, P. G. 1991, *ApJ*, 377, 210
- Rodríguez, L. F., García-Barreto, J. A., & Gómez, Y. 1985, *Rev. Mexicana Astron. Astrofis.*, 11, 109
- Roelfsema, P. R., & Goss, W. M. 1992, *A&A Rev.*, 4, 161
- Roelfsema, P. R., Goss, W. M., Zijlstra, A. A., & Pottasch, S. R. 1991, *A&A*, 251, 611
- Spitzer, L. 1978, *Physical Processes in the Interstellar Medium* (New York: John Wiley & Sons)
- Steffen, W., & López, J. A. 1998, *ApJ*, 580, 696
- Zijlstra, A. A., Pottasch, S. R., & Bignell, C. 1989, *A&AS*, 79, 329